Carbon 119 (2017) 535–543

Contents lists available at ScienceDirect

Carbon

journal homepage: www.elsevier.com/locate/carbon

High-quality PVD graphene growth by fullerene decomposition on Cu foils

J. Azpeitia [a], G. Otero-Irurueta [b], I. Palacio [a], J.I. Martinez [a], N. Ruiz del Árbol [a], G. Santoro [a], A. Gutiérrez [c], L. Aballe [d], M. Foerster [d], M. Kalbac [e], V. Vales [e], F.J. Mompeán [a], M. García-Hernández [a], J.A. Martín-Gago [a], C. Munuera [a], M.F. López [a, *]

[a] Materials Science Factory, Instituto de Ciencia de Materiales de Madrid (ICMM-CSIC), Sor Juana Inés de la Cruz 3, E-28049, Madrid, Spain
[b] Center for Mechanical Technology and Automation (TEMA-DEM), University of Aveiro, 3810-193, Aveiro, Portugal
[c] Departamento de Física Aplicada, Universidad Autónoma de Madrid, E-28049, Madrid, Spain
[d] ALBA Synchrotron Light Facility, Carrer de la llum 2-26, Cerdanyola del Vallès, Barcelona, 08290, Spain
[e] J. Heyrovský Institute of Physical Chemistry, ASCR, v.v.i., Dolejškova 3, CZ-18223, Prague 8, Czech Republic

ARTICLE INFO

Article history:
Received 1 March 2017
Accepted 25 April 2017
Available online 3 May 2017

ABSTRACT

We present a new protocol to grow large-area, high-quality single-layer graphene on Cu foils at relatively low temperatures. We use C_{60} molecules evaporated in ultra high vacuum conditions as carbon source. This clean environment results in a strong reduction of oxygen-containing groups as depicted by X-ray photoelectron spectroscopy (XPS). Unzipping of C_{60} is thermally promoted by annealing the substrate at 800 °C during evaporation. The graphene layer extends over areas larger than the Cu crystallite size, although it is changing its orientation with respect to the surface in the wrinkles and grain boundaries, producing a modulated ring in the low energy electron diffraction (LEED) pattern. This protocol is a self-limiting process leading exclusively to one single graphene layer. Raman spectroscopy confirms the high quality of the grown graphene. This layer exhibits an unperturbed Dirac-cone with a clear n-doping of 0.77 eV, which is caused by the interaction between graphene and substrate. Density functional theory (DFT) calculations show that this interaction can be induced by a coupling between graphene and substrate at specific points of the structure leading to a local sp^3 configuration, which also contribute to the D-band in the Raman spectra.

1. Introduction

After the major impact that graphene produced on the scientific community because of its diverse and exceptional properties (high carrier mobility, high elasticity, chemical inertness, high thermal conductivity, tunable band gap, half-integer quantum Hall effect, etc.) [1], the focus is currently placed on its promising technological applications. Many different experimental protocols have been established to achieve a controlled, scalable and low-cost production of this carbon allotrope, though still a single formula combining all the aforementioned aspects is lacking [2]. Although exfoliation of graphene from graphite, the pioneering method used by Geim and coworkers [3], led to numerous exciting discoveries of graphene electronic and mechanical properties [4,5], the lack of scalability of this protocol has motivated the exploration of other preparation methods involving different types of precursors and substrates [6–9]. Undoubtedly, the most extended method has been graphene growth on metal substrates by chemical vapor deposition (CVD) using hydrocarbon gaseous reactants such as methane, acetylene or ethylene [10]. However, the current CVD processes usually require elevated temperatures (around 1000 °C) to decompose the gaseous reactant and to succeed in the graphene formation procedure. In order to overcome the temperature drawback of this method, many efforts have been made to lower these values in the search of a cost efficient and environmentally friendly route.

In this work, we have explored a different graphene synthesis methodology taking advantage of the knowledge and technology that surface science provides. As substrate, copper in the form of foil was chosen due to its low carbon solubility, catalytic-like action and low price. As carbon source, C_{60} molecules were used [11],

* Corresponding author.
E-mail address: mflopez@icmm.csic.es (M.F. López).

http://dx.doi.org/10.1016/j.carbon.2017.04.067
0008-6223/

which represent an optimal choice, since they only contain the desired chemical element in graphene growth, together with their relative low cost and highest abundance among fullerenes. The C_{60} molecules, although stable at room temperature, decompose upon annealing at temperatures beyond 700 °C [12]. For this reason, it is expected that not extremely high temperatures will be needed to favor the chemical reaction for growing graphene from C_{60} molecules, making this new route advantageous.

Indeed, the transformation of C_{60} into graphene was previously reported on Ni thin films, Pt(111), Ru(0001) and Ir(111) surfaces, in which the metal-catalyzed cage-opening of C_{60} was achieved in the 700–1000 °C temperature range [13–16]. All the above systems fall into the category of strongly interacting interfaces, in which C_{60} adsorption is dominated by molecule-substrate interaction rather than intermolecular interactions. In fact, for these systems several studies agree that the C_{60}-surface interaction induces the formation of surface vacancies, increasing the substrate–carbon bonding strength [15,17,18]. This would explain why annealing at elevated temperatures does not cause desorption of the molecule (as observed for other metal surfaces) but rather C_{60} fragmentation and subsequent graphene formation.

Less explored is the conversion from C_{60} to graphene on not so strongly interacting interfaces. It is particularly striking that, being one of the most employed substrates in the widely used CVD growth method, to our knowledge only two works have reported the attempt to grow graphene from C_{60} on copper, with dissimilar results. Yamada and collaborators did not succeed in inducing C_{60} cage unzipping on Cu(111) upon annealing up to 580 °C, reporting the formation of disordered clusters on the surface due to molecular polymerization [14]. Very recently, Tatti and co-workers [19] reported the synthesis of graphene on copper by C_{60} supersonic molecular beam epitaxy (SuMBE). The quality of the resulting graphene, however, is far from the aforementioned C_{60}-derived counterparts, with the presence of pentagons and vacancies and a small coherence length that even hinders the formation of a low energy electron diffraction (LEED) pattern [19].

In the present work, we describe the successful growth of high quality graphene by directly evaporating C_{60} molecules on thin polycrystalline copper substrates at 800 °C in ultra-high vacuum (UHV) conditions. Working in this controlled environment allows keeping the surface clean for several hours, enough for exploiting the catalytic-like properties of the metallic substrate when exposed to the adequate organic precursor. Several in-situ and ex-situ surface and spectroscopic techniques have been employed for the characterization of the synthesized graphene. With a few exceptions, characterization of graphene grown on copper foil is commonly performed once transferred to Si/SiO_2 substrates, since direct characterization on polycrystalline foils poses several difficulties, such as high surface roughness, detrimental for scanning microscopy characterization, or much lower Raman scattering intensity and higher spectral background. However, transfer processes might modify some of the properties of the grown graphene. Therefore, in the present work, LEED, X-ray photoelectron spectroscopy (XPS), angle resolved photoemission spectroscopy (ARPES), electron backscatter diffraction (EBSD), scanning electron microscopy (SEM), atomic force microscopy (AFM), X-ray diffraction (XRD) and Raman spectroscopy measurements were directly performed on the as-grown samples, i.e., without transferring the graphene to a different substrate, so as to obtain a thorough characterization of the C_{60}-derived graphene, despite the inherent difficulties. Additionally, theoretical calculations were performed in order to understand some basic points of the surface-graphene interaction. These results indicate that the proposed route provides high quality large area single-layer graphene on a technologically relevant substrate, such as polycrystalline copper, at a lower temperature than that used in conventional CVD.

2. Experimental and theoretical details

In order to investigate the main characteristics of the graphene layer grown by using C_{60} molecules, different polycrystalline Cu surfaces were studied. Cu foil 25 μm thick (Alfa Aesar, 99.8% purity), Cu foil 50 μm thick (Alfa Aesar, 99.8% purity) and Cu foil 1.27 mm (Alfa Aesar, 99.9% purity) were used as substrates. The main drawback of the 25 μm foil was the occasional bending of the surface by the effect of the temperature. Except for those infrequent cases, the results were similar for all substrates. The surface of the Cu substrate was prepared by following a standard cleaning procedure in an UHV chamber (base pressure 3×10^{-10} mbar) consisting of successive cycles of argon sputtering and thermal annealing at 800 °C. The substrate temperature was monitored with an optical pyrometer. Commercial C_{60} molecules (Sigma Aldrich, 98% purity) were used as precursor species for growing graphene on the substrate. These fullerenes were evaporated directly in the UHV system using a home-made evaporator based on a tantalum crucible. Prior to the experiments, C_{60} molecules were purified for several hours at 500 °C. During graphene growth, C_{60} molecules were evaporated in UHV at a sublimation temperature of 450 °C. As a preparation of the procedure, the clean Cu foil was heated up to 800 °C and kept at this temperature. Then, the fullerene molecules were sublimated onto the hot substrate during typically 1 h. CVD graphene was grown on copper for comparative purposes. Copper foil was exposed to a hydrogen atmosphere and heated to 1000 °C. At this temperature, the substrate was annealed under the hydrogen flow of 50 standard cubic centimeters per minute for 20 min, when the methane precursor was applied. The CVD process with the mixture of H_2 (50 sccm) and CH_4 (1 sccm) gases was carried out for 30 min and an additional 5 min of pure hydrogen flow allowed etching of the top of the layers. Then, the sample was cooled to 90 °C and removed from the reactor. The pressure of the precursors (either the H_2–CH_4 mixture or only hydrogen) was kept constant at a value of 350 mTorr during the whole growth process.

The cleanliness of the substrate was checked by LEED, which allowed the observation of different spots corresponding to the different Cu crystallographic orientations. Moreover, some control substrates were chosen after the cleaning treatment to study their surface morphology by AFM and verify the lack of contamination. An increase in grain size together with the development of flat terraces was also observed after substrate cleaning. After growth, LEED patterns were used to check *in situ* graphene formation on the sample surface. At this stage, the sample was taken out of the UHV chamber to perform the structural and morphological characterization of the graphene layer. For this purpose, a commercial AFM system and software (WSxM) from Nanotec [20] operating in ambient conditions was employed. Topographic images were acquired in dynamic mode, exciting the tip at its resonance frequency (~75 kHz in our case). Commercial AFM tips from Next-Tip S.L. [21] were used. Raman spectra were collected with a confocal Raman microscope (Witec alpha-300R) equipped with a 532 nm excitation laser and a 100x objective lens (NA = 0.9). The optical diffraction resolution of the confocal microscope was limited to about ~400 nm laterally. The incident laser power density was lower than 40 $mW/\mu m^2$, below the onset of sample damage. SEM micrographs were recorded on a FEI Nova NanoSEM 230 microscope using a vCD detector. XPS spectra were recorded with a VG-CLAM hemispherical electron energy analyzer using Mg Kα radiation (1253.6 eV) in an UHV chamber with a base pressure lower than 10^{-9} mbar. XRD θ-2θ patterns were measured using a BRUKER 4-circle thin film

diffractometer operating on Cu $K\alpha_1$ radiation ($\lambda = 0.154056$ nm) in a nearly-parallel beam configuration. The EBSD orientation maps were recorded using a Hitachi S4800 scanning electron microscope operated at 20 keV with the sample tilted by 70°. The mapping was performed with a lateral step of 2 μm. ARPES experiments were performed at the CASSIOPÉE beamline (SOLEIL synchrotron, France) with a hemispherical photoelectron spectrometer (VG Scienta R4000). The spectra were measured at room temperature using a photon energy of 36 eV with a beam spot size ranging from 40×20 to 100×100 μm^2 and in a UHV system with a base pressure in the range of 10^{-10} mbar. Finally, μ-LEED patterns were acquired at the LEEM-PEEM experimental station of the CIRCE beamline at ALBA Synchrotron [22] using an illumination aperture of 10 μm diameter on selected areas of an *in situ* grown sample.

We have computed the Gr/Cu(110) interface by DFT [23] calculations implemented in the plane-wave code QUANTUM ESPRESSO [24]. In particular the vibrational modes of pristine graphene and graphene on that surface have been calculated using an efficient approach based on a second order response to DFT. This result can be regarded as a crude estimation of the non-resonant contribution to the Raman spectrum. For that purpose we computed the second order derivative of the electronic density matrix with respect to a uniform electric field, using pseudopotentials and periodic boundary conditions (see Refs. [25–30]). To establish the optimal ground-state, interfacial configurations, total energies, forces, and stresses were minimized (for both structure and lattice) by using DFT [24], considering a perturbative van der Waals (vdW) correction to account for dispersive forces [31,32]. A generalized gradient approximation parametrization [33] was used for the exchange-correlation potential, and norm-conserving Troullier-Martins pseudopotentials to model the ion–electron interaction [34]. All the Brillouin zones were sampled by means of optimal Monkhorst-Pack grids [35], using a kinetic energy cutoff of 40 Ry to guarantee a full convergence in energy and electronic density. For the calculation of phonon modes we considered a $(4 \times 4 \times 1)$ k-points grid. A description of the geometrical model is explained in detail in the supplementary information (see Fig. S5).

3. Results

LEED patterns were used to determine the crystallinity and cleanliness of the substrate. The as-received Cu foil does not show any LEED spot, indicating that the surface is oxidized. However, after successive sputtering-annealing cycles of the substrate in UHV there is a thermally promoted recrystallization process, which leads to a notorious increase of the grain sizes and the appearance of bright and well-focused spots at the LEED pattern (see Fig. S1 of the supplementary information). The crystallographic configuration was different from one Cu foil sample or region to another, indicating a smaller grain-size than the electron beam spot and that there is not a common geometrical orientation. In our case the electron beam size of our LEED equipment is within the sub-millimeter range, and considering that just few spots are seen, this indicates that just a few crystallites are sampled by the electron gun, and therefore they should have an approximate size of tens of microns, in good match with the AFM images shown below.

On this kind of substrate the graphene growth protocol was followed (see experimental details). Although LEED patterns were recorded routinely at the laboratory, after determination of the best experimental conditions for the growth method also μ-LEED experiments were performed at the ALBA synchrotron. Fig. 1a represents a typical μ-LEED pattern obtained after graphene growth on the Cu foil surface. As can be observed, the μ-LEED pattern acquired at 40 eV shows a ring of modulated intensity and multiple bright spots mainly in square or rectangular geometries. The ring is the fingerprint of a polycrystalline graphene layer and arises from the superposition of hexagonal patterns from rotated graphene domains, as its radius with respect to the (00) spot corresponds to the graphene lattice parameter (0.246 nm). Moreover, the modulation of the graphene ring indicates that some of the graphene orientations appear more frequently than others, which is related to the larger stability of some particular graphene orientations with respect to the surface (known as Moiré superstructure in single crystal surfaces) [36]. This pattern is observed along the whole sample surface evidencing the formation of a continuous graphene layer. On the other hand, the multiple bright spots, which are observed in addition to the ring, exhibit mainly rectangular crystallographic order, corresponding to Cu(110) grains. This result contrasts with the LEED pattern reported for graphene grown by CVD on Cu foils. In that case, the main crystallographic orientation of the Cu grains is hexagonal [37], corresponding to Cu(111) grains.

EBSD measurements also corroborate this difference in preferred crystallographic orientation of the copper grains, depending on the growth method. Fig. 1c and d show representative EBSD orientation maps of graphene grown on Cu by different methodologies, and the inset in Fig. 1d exhibits the color code assignment for the different Cu lattice orientations. Fig. 1c corresponds to a Cu foil in which graphene has been grown using our protocol based on low-temperature decomposition of C_{60}. The image exhibits multiple grains with different crystal orientations. However, the (110) orientation seems to dominate. On the other hand, Fig. 1d represents the EBSD orientation map for the case of the CVD graphene grown sample (see experimental details). In this case, the most prevailing orientation for the multiple grains is (111). Though the particular grain crystallographic distribution differs from sample to sample, the average orientation is representative of all samples grown with the two different methodologies. The different behavior of the Cu foil itself obtained for the two graphene formation methods is remarkable. In fact, this result is in agreement with the LEED observation. One plausible explanation is based on the temperature used in each process. The higher temperatures used for CVD growth could be responsible for the formation of (111) grains [38] while the lower temperatures used in the C_{60} based procedure may lead to the formation of mainly (110)-type Cu grains. In order to gain insight into the crystal orientation prevalence of the substrate, XRD patterns were obtained from Cu foils which have undergone the same pre-growth treatment protocol but which have been taken out of the vacuum chamber just before the graphene growth (see Fig. 1b). The black peaks on this figure represent the experimental diffraction data and the red bars the excess ratios with respect to normalized ideal powder intensities. Those excess ratios are obtained by dividing the experimental intensity by the ideal powder intensity for each reflection and the resulting value is then normalized to the (111)-reflection intensity. Thus, Fig. 1b evidences an abnormal pattern in the observed diffraction peak intensities by comparison with the powder average and after normalisation to the intensity of the (111) reflection: there is an increase by factors 7, 9 and 13 of the observed intensities for the (311), (200) and (220) reflections, respectively. The latter we interpret as an increase in the number of (110) oriented grains. In that case, the temperature used for the cleaning process was 800 °C, i.e. the same as that used for the graphene growth method and much lower than the typical temperature used in CVD processes. This is a remarkable finding, due to the important role of the substrate lattice orientation in the growth process, as reported by Kalbac [39].

The top images of Fig. 2 show the morphology of the sample surface measured by AFM. AFM images are recorded on a single Cu crystallite or grain, and the presence of different atomic steps delimiting terraces tell us that the substrate was atomically clean

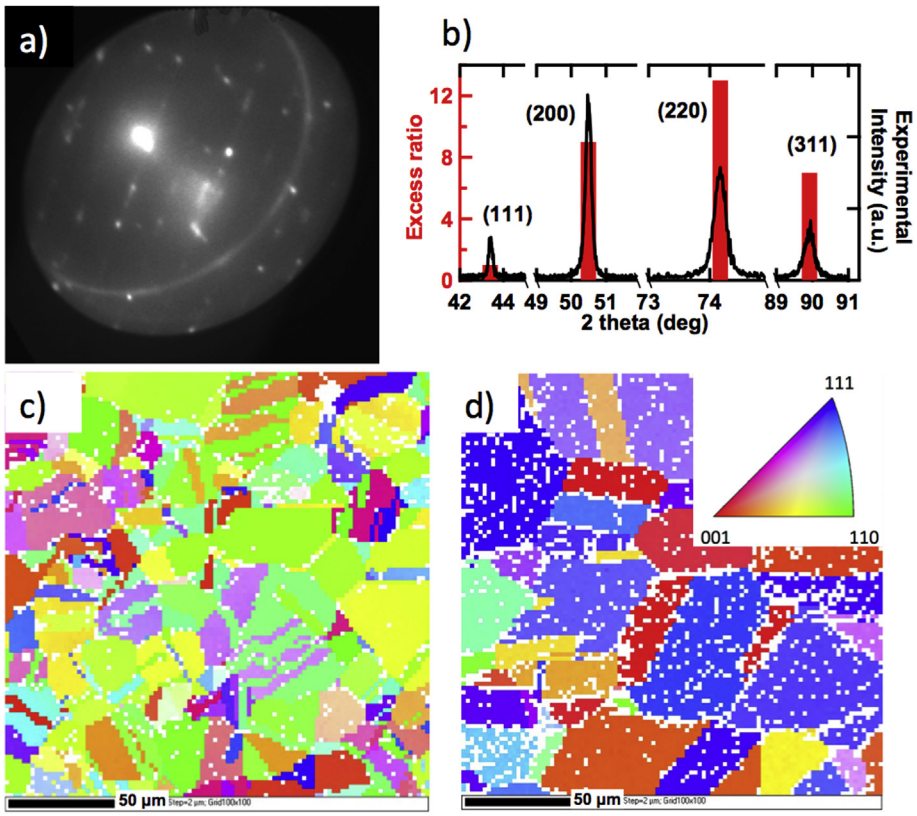

Fig. 1. a) μ-LEED pattern obtained after graphene grown on the Cu foil surface taken at 40 eV b) XRD diffraction pattern shows experimental and excess ratios with respect to normalized ideal powder intensities (black curves and red bars, respectively) indicating a predominance of the (110) orientation. c) EBSD orientation map for a Cu foil after growing one monolayer of graphene by using C_{60}. d) EBSD for a Cu foil with CVD graphene. The inset shows the color code assignment for the different lattice orientation. (A colour version of this figure can be viewed online.)

before the growth process. In the AFM images the presence of the graphene layer is indirectly detected by the formation of the characteristic wrinkles that appear in graphene due to stress caused by the differences in the thermal expansion coefficients of graphene and copper. These wrinkles are observed to cross the substrate terraces, indicating that structurally coherent regions of graphene extend beyond the steps. The length of these wrinkles is no longer than one micron, which is shorter than the values reported in the literature [40], and probably related to the lower growth temperature. Wrinkles are usually linked to graphene boundaries and consequently, these topological defects are a good indication of the graphene layer formation on the metallic substrate. From a close inspection of the AFM images, one can realize that in our case wrinkles do not define a closed area, but leave open paths all over the surface, indicating that the extension of graphene is larger than the Cu grain size. In the inset image a height profile corresponding to one of the wrinkles can be observed. The typical width of the substrate terraces is of the order of hundred nanometers. In some of the wrinkles or grain boundaries the graphene could change the relative orientation with respect to the substrate, increasing the number of different rotational domains, and also contributing to the diffraction ring seen in μ-LEED (see Fig. 1a).

The bottom images of Fig. 2 show SEM micrographs for the special case of a Cu foil substrate partially covered by graphene, where the presence of several Cu grains with a typical width of tens of microns can be observed. The growth of this incomplete graphene layer was performed with the aim of studying the graphene morphology before the formation of the complete monolayer (about 0.8 ML). In this particular case, we checked that uncovered Cu areas appear lighter than those from graphene in the SEM image. The boundaries between Cu grains are clearly observed (see also Fig. S2). Interestingly, in some cases the graphene layer crosses the boundaries between neighboring Cu crystallographic domains, extending over different Cu grains, as it is shown in the encircled regions in the right bottom micrograph of Fig. 2. These areas show that graphene growth is not confined to the crystallographic grain where nucleation starts, but extends to neighboring grains. In the case of completed graphene layers (Fig. S2b of the supplementary information), such a contrast associated with graphene was not observed by SEM and only the morphology of the Cu grains could be distinguished.

To determine the influence of the cleaning and growth procedures on the substrate morphology, roughness analysis was performed on the as-received Cu foil, the treated Cu foil and the foil with graphene grown on top. The root mean square (RMS) roughness value, calculated for 500×500 nm^2 areas, is 1.2 nm for the as-received foil, decreases to 0.4 nm after the UHV cleaning procedure and remains constant after graphene growth (see Fig. S3). Excluding wrinkles, the AFM images show a uniform graphene layer covering the copper terraces, with no evidence of the presence of bilayer or multilayer patches. Most previous works reported that the advantage of using copper as substrate for graphene formation, beyond its low cost, is related to the low solubility of carbon into the bulk, conferring a quasi self-limiting character to the growth. Attending to the binary phase diagram of Cu–C [41], the carbon solubility in Cu decreases with decreasing temperature, being around 0.002% at 800 °C, in contrast to typical CVD temperatures around 1050 °C, where the solubility is four times larger.

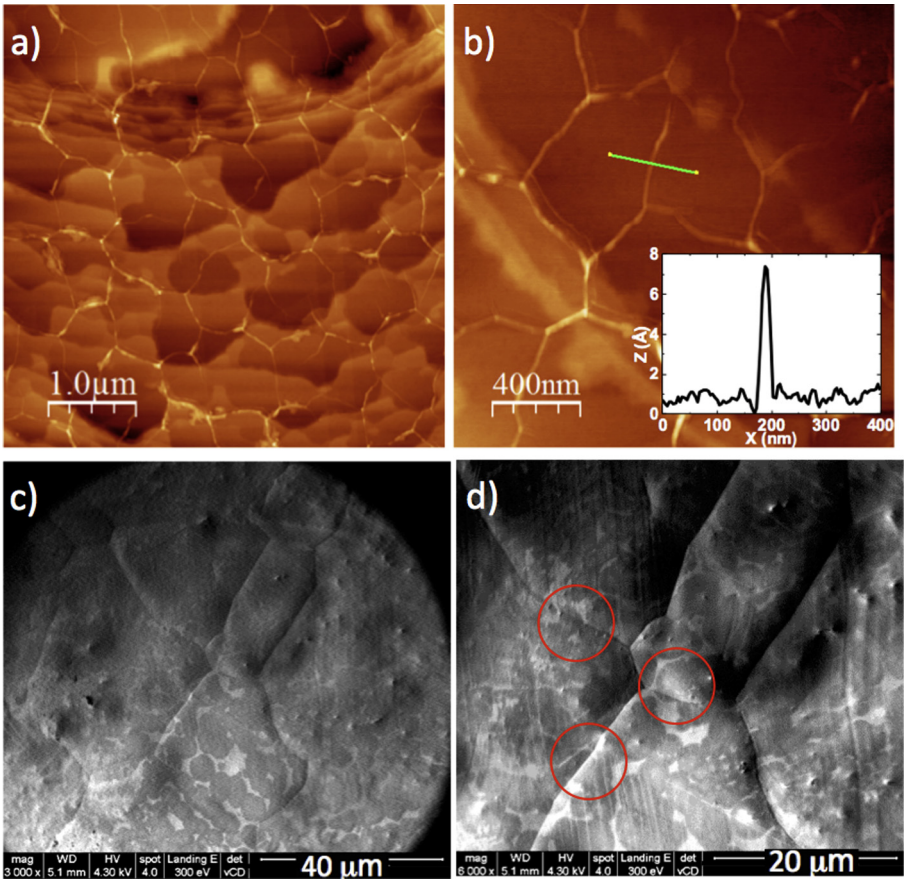

Fig. 2. Top: AFM images of the graphene layer grown on the Cu foil by the decomposition of C_{60} molecules. The characteristic wrinkles of graphene are observed crossing across the Cu terraces and grains. The inset shows a height profile corresponding to one of the wrinkles. Bottom: SEM images of an incomplete graphene layer (0.8 ML) showing the boundaries between larger Cu grains. The uncovered Cu areas appear lighter than the graphene. The red circles highlight regions where graphene nucleation extends over adjacent Cu grains. (A colour version of this figure can be viewed online.)

Besides this low carbon solubility values at the temperature used in our growth process, the low pressure conditions of the C_{60} thermal deposition also contribute to the creation of only one monolayer of graphene. As we will see below, in addition to the AFM measurements, different experimental techniques used in the present study reveal the formation of a single graphene monolayer, which suggests a self-limiting mechanism in the catalytic-like action of Cu.

XPS measurements were carried out to identify the chemical species on the sample surface. XPS analyses were performed ex-situ: after growing the graphene layer on the Cu foil substrate under UHV conditions, the sample was exposed to air in order to transfer it to the XPS equipment. Fig. 3 shows an XPS C-1s spectrum of a graphene layer grown on the Cu foil using C_{60} as precursor. It is important to mention that the sample was measured without any cleaning treatment before the XPS data acquisition. To determine the different components of the C-1s emission, the XPS spectrum was fitted using standard Gaussian-Lorentzian lines and the corresponding integral background. In order to accommodate the typical asymmetric line shape of sp^2 carbon, this component was fitted using a Doniach and Sunjic line shape with an asymmetry parameter of 0.068 [42]. The solid black line through the data points represents the result of the least-squares fit. Five components were used to simulate the emissions corresponding to the different chemical environment of the carbon atoms. Thus, the subspectra located at 284.4, 285.4, 286.7, 288.5 and 290.5 eV, are assigned to C-sp^2, C–OH, C–O, C=O, and C–C=O together with O–C=O species, respectively. The strong intensity of the C-sp^2 component with respect to the oxide components evidences, even after air exposure, the high quality of the graphene. In most cases of graphene layers grown by CVD, the XPS intensities corresponding

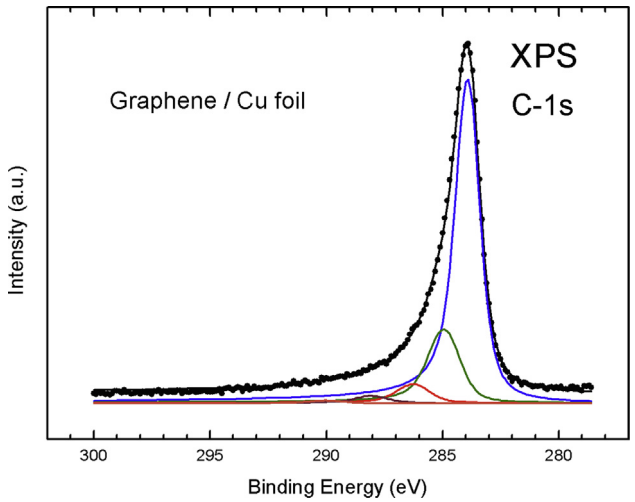

Fig. 3. XPS C-1s core level spectrum (black dots) of the graphene layer on the Cu foil. The main subspectrum corresponds to the sp^2 carbon emission. (A colour version of this figure can be viewed online.)

to the oxygen-rich species are larger than those observed here, which indicates a higher presence of oxygen-containing groups in those CVD samples [43]. In our case, the combination of UHV conditions and low temperatures involved in the growth process, which prevents segregation of many of the contaminants contained in the copper bulk ensures a controlled and cleaner procedure. The oxide components in the XPS spectrum are probably coming from the exposure of the sample to air. It is worth mentioning that the XPS technique does not allow distinguishing whether some unbroken C_{60} molecules are present on the surface, because the C-sp^2 C_{60} emission from such species undergoes a very small shift, around 0.06 eV [36], with respect to the C-sp^2 graphene signal, which is below the resolution of the equipment.

The ultimate evidence for single-layer graphene synthesis is generally given by Raman spectroscopy. Previous to the Raman data acquisition, images of the graphene/Cu sample were taken with a 100 × optical confocal microscope, showing copper grains, with sizes of the order of tens of microns, as can be seen in a typical image shown in the inset of Fig. 4. This, again, confirms the increase of the mean Cu grain size due to the recrystallization process induced by the annealing treatment, and agrees with the observation of multiple spots in the LEED patterns shown in Fig. 1a. The Raman measurements were performed on different regions of the samples to check the uniformity of the graphene layer. A representative spectrum of a freshly prepared sample is shown at the lower curve of Fig. 4, in red color. It exhibits the G, 2D and D peaks that are distinctive of graphene although with very reduced intensity. Similar low intensity Raman spectra have been observed for graphene epitaxially grown on single crystals [44] and has been interpreted as a quenching of the vibrational spectral features. The upper black curve presents the Raman spectrum of the same sample, taken two months after growth. In this time the sample was exposed to air under ambient laboratory conditions (at temperatures varying between 18 °C and 30 °C and relative humidity values between 20% and 60%). Surprisingly the peaks have now a much larger intensity, though no visible changes are observed in the morphology of the sample measured with AFM indicating that the measured intensity enhancement is most likely related to the evolution of the graphene-copper interface. A similar enhancement has been observed in graphene on copper foils exposed to air, and has been related to the formation of copper oxide and to the intercalation of molecules from the atmosphere through defects in the graphene lattice [45,46]. Additional experiments, beyond the scope of this work, are being carried out by us to investigate in a more controlled manner this effect, which certainly points out to a decoupling of the graphene layer from the copper substrate due to ambient molecular intercalation, resulting in an enhanced Raman signal due to the reduction of electromagnetic screening from the copper substrate [47]. The intensity and position of the 2D peak are generally used to gather information on the number of graphene layers. For monolayer graphene, a single peak with full-width-half-maximum (FWHM) ~30 cm^{-1} and normalized intensity (I_{2D}/I_G) > 1 (<1 for multilayers) is expected [48]. From the black curve in Fig. 4, an intense 2D peak is observed at 2689 cm^{-1}. The spectral shape of the 2D peak is quite narrow, with a FWHM of 26.6 cm^{-1} (as adjusted with a Voigt profile), and highly symmetric, i.e., it is made of a single component, as is the case for monolayer graphene. The calculated integrated I_{2D}/I_G ratio gives a value of 5.2, which corroborates the previous observation of the presence of a monolayer of graphene. On the other hand, the G peak, located at 1594 cm^{-1}, exhibits a FWHM of 15.6 cm^{-1}. All these values fall within the typical range of values established for a graphene monolayer not significantly subjected to strain [49].

Additionally, a small D peak was also detected at 1351 cm^{-1} with a FWHM of 15.6 cm^{-1}. The D peak is, however, less intense than the one found in a previous work on C_{60} decomposition on nickel where, due to the strong D signal, the possibility of improving the quality of the graphene layer by using another metallic substrate or another precursor was suggested [13]. Raman spectra collected at different points of the sample showed that the monolayer of graphene uniformly covers the copper foil surface (see Fig. S4).

In our experimental protocol, graphene grows on a previously UHV cleaned Cu polycrystalline substrate with a certain (110) texture. Under these conditions a strong coupling between the metal surface and graphene can be expected. To gain some insight into the interactions at the interface, we have performed theoretical calculations of the vibrational modes of free-standing graphene and of Gr/Cu(110), which can be considered as a crude approximation to the Raman spectrum, excluding the well-known Raman resonant processes in graphene as well as two-phonon phenomena. The results of the DFT structural optimization reveal that the interaction of the graphene with the metal substrate strongly depends on the surface configuration. The optimization of the simulation cell leads to a buckled graphene surface due to the interaction of some distinct C atoms with the Cu atoms underneath, inducing a corrugation on the graphene layer of about 0.22 Å for Gr/Cu(110). At these particular points the C atom is displaced towards the Cu surface, interacting more strongly with the Cu, thus acquiring a sp^3 character. Fig. 5 shows that the calculation of the vibrational modes for free-standing graphene presents, as expected when excluding anharmonic effects, a unique feature at 1599 cm^{-1}, characteristic of sp^2 carbon, that can be assigned to the well-known G band. When the graphene layer is simulated on the Cu(110) surface (see details in the supplementary information), a new feature appears at 1365 cm^{-1} due to interaction with the substrate. Our calculations show that the graphene-substrate interaction may induce the rupture of the sp^2 hybridization producing the appearance of local regions with sp^3 character [50] and a diamond-like sp^3 vibrational band, whose frequency lies in the same spectral region as the graphene D band characteristic of structural defects (Fig. 5). Therefore, in our case, in addition to a D band accounting for structural defects at grain boundaries or graphene wrinkles, the aforementioned sp^3 carbon hybridization due to the interaction with the Cu surface could also contribute to this spectral feature.

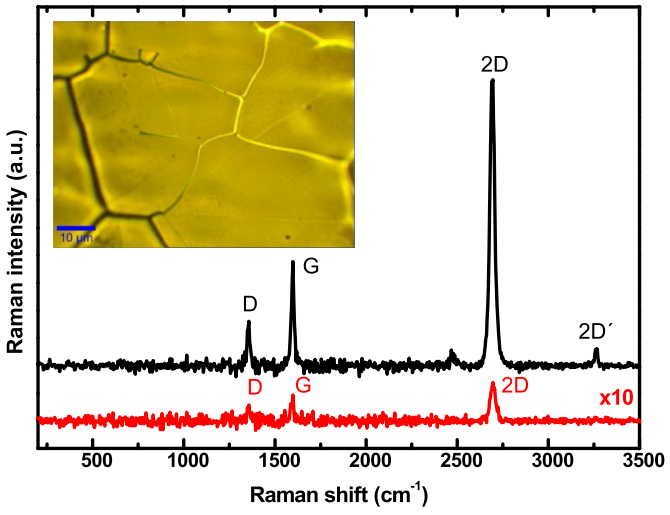

Fig. 4. Representative Raman spectra, taken with a laser wavelength of 532 nm. The red spectrum at the bottom was obtained just after the graphene growth while the black spectrum at the top corresponds to aged graphene. A sharp 2D band is observed together with less intense D and G bands. The inset shows a 100 × optical image taken on the graphene grown surface, where the copper substrate grains are visible. (A colour version of this figure can be viewed online.)

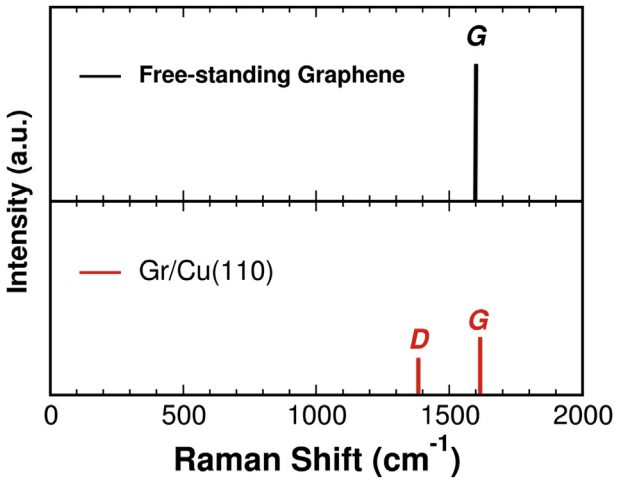

Fig. 5. First approximation of the theoretical calculation of the Raman scattering for free standing graphene and graphene on Cu(110). The G band is visible in both cases while the D band emerges for the graphene layer on top of a Cu(110) surface. (A colour version of this figure can be viewed online.)

Nevertheless, even though we may have an extra contribution to the D band in the Raman spectra, our D intensity (Fig. 4) is comparable to that already published [51].

The experimental conditions for the CVD growth of graphene do not exclude the presence of oxide species below the graphene layer, which would favor a decoupling with the substrate. However, in our physical vapor deposition (PVD) methodology, as we have already mentioned, no Cu oxides were detected in the samples. In our case, the clean Cu atoms in the terraces are prone to react with C atoms from the graphene, favoring strong coupling at specific locations and doping as will be shown next.

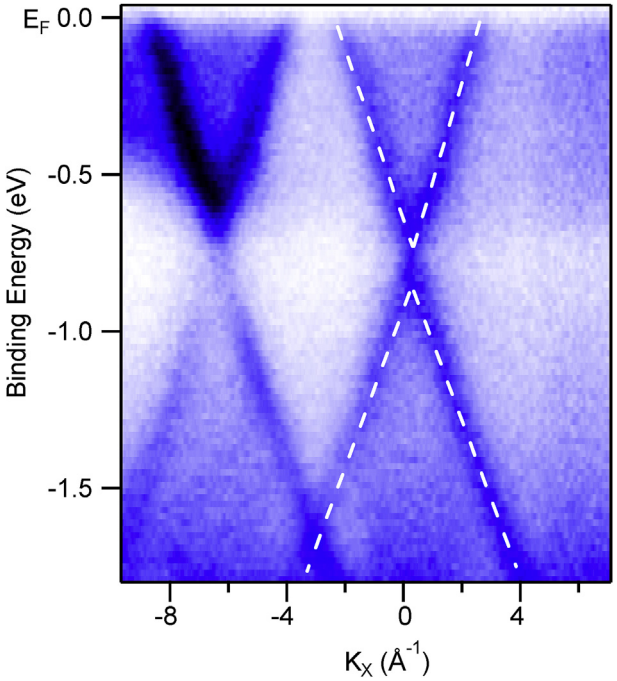

Fig. 6. Energy-momentum dispersion of a multi-grain graphene layer on a Cu foil measured with circularly polarized light of 36 eV in the vicinity of K point along K_x direction. Due to the contribution of different graphene grains more than one band is observed. (A colour version of this figure can be viewed online.)

The electronic structure of our single layer graphene was also investigated by means of ARPES. Fig. 6 shows a multigrain photoemission momentum map along K_x direction of the sample using circularly polarized light of 36 eV. In this case and due to the polycrystalline nature of our sample, the photoemission data taken along any ΓK direction will show not only one Dirac cone but multiple π bands. That is the case in Fig. 6, where the two Dirac cones are observed in the image, corresponding to two adjacent graphene grains. The right one (labeled as $K_x = 0$ Å^{-1}) is exactly at one K point whereas the one near $K_x = -6$ Å^{-1} is slightly misaligned, and therefore it should not be taken into account to study the doping and the gap of this sample. It can be clearly observed that the electronic bands are completely linear, as corresponds to a massless Dirac fermion behavior. A deeper study of the data show an n-type doping of 0.77 eV, which is probably due to the coupling of the graphene π bands and the copper d-band [52]. In fact, n-doping agrees with the Raman data, where the G peak position at 1594 cm^{-1} corresponds to a negative charge carrier concentration [53]. This result differs from previous observations of graphene grown by CVD on Cu foil, where a lighter doping, around 0.4 eV [37,54], or even an undoped [55] behavior was found. This difference can be ascribed to the present growth procedure, involving UHV conditions, clean surface, C_{60} molecules and complete single layer graphene, which leads to a larger coupling between graphene and the substrate, as the theoretical calculations suggest. This coupling would also be responsible for the charge transfer from the Cu foil to the graphene layer. In this sense, gaps of 0.36 eV have been reported for graphene on Cu in UHV [52]. Moreover, our ARPES data also evidence the existence of a small bandgap of 0.12 eV, which is in the range of other gaps already reported for similar systems [37,52]. Finally, Fig. 6 does not show parabolic bands, typical of the presence of bilayer graphene or graphene oxide regions, indicating the growth of an extended single layer graphene in agreement to the Raman and AFM data, and the prevalence of the graphene electronic properties on this technologically relevant kind of samples.

4. Discussion and conclusions

In this work, large area graphene monolayer was grown on Cu foils in UHV conditions using C_{60} as precursor molecules. The mechanism of graphene layer formation on the Cu surface is based on the decomposition of the C_{60} molecules, a thermally activated process promoted by the Cu surface. The above-mentioned process presents several advantages with respect to the use of hydrocarbons as carbon sources. First, the process is self-limiting and only single layers are obtained. Second, it requires lower substrate temperature than conventional CVD graphene growth methods. The decrease of the temperature results in two main advantages: on the one hand, fewer impurities are segregated to the surface, promoting an ultra-pure graphene-copper interface, and on the other hand the solubility of carbon into the Cu bulk is reduced, avoiding the formation of bilayer or few layer domains in the graphene layer. Moreover, in our experimental protocol UHV conditions were used, and therefore, the surface was atomically clean before experiments, so no oxygen was involved or intercalated during the process.

With the aim of evaluating the quality and properties of the graphene layer, different characterization techniques were applied on the as-grown samples. The in-situ LEED pattern of the Cu foils after the surface cleaning process showed characteristic spots of different Cu facets, which corresponds to a typical polycrystalline specimen. After graphene growth, a clear ring feature appears in the in-situ LEED pattern, evidencing the presence of a multidomain graphene film on the surface, although some graphene orientations

prevail. The morphology of the graphene layer was studied by ex-situ AFM. The AFM images exhibited complete coverage of the areas measured and uniform graphene film on the Cu foil. The presence of graphene wrinkles, crossing the substrate terraces, was also observed. Raman spectra, similar along the sample surface, showed a narrow 2D band as well as G and D peaks. By investigating the surface chemical composition by XPS, sp^2 hybridized carbon emission is the main contribution and only low contents in functional groups were observed after exposing the sample to atmospheric conditions. ARPES measurements showed that the band structure of graphene grown on the Cu foil is based on multiple linearly dispersing graphene bands, which correspond to different graphene grains. All results suggest that the envisaged protocol to synthesize graphene from C_{60} molecules is a successful strategy to obtain large area uniform single layer graphene on technologically relevant substrates at lower temperature than the widespread CVD method.

Acknowledgements

Financial support from EU Horizon 2020 research and innovation program under grant agreement No. 696656 (GrapheneCore1-Graphene-based disruptive technologies) and Spanish MINECO (grants MAT2014-54231-C4-1-P,MAT2014-52405-C2-2-R, CSD2009-00013, MAT2015-64110) is acknowledged. JA and NR are supported by the FPI program from MINECO (BES-2012-058600 and BES-2015-072642, respectively). CM and JIM acknowledge the financial support by the "Ramón y Cajal" Program of MINECO (RYC-2014-16626 and RYC-2015-17730, respectively). JIM and GS acknowledge funding from the ERC-Synergy Program (grant ERC-2013-SYG-610256 Nanocosmos). JIM thanks CTI-CSIC for use of computing resources. MK and VV acknowledge funding from ERC-CZ (LL1301) project. GO-I acknowledges FCT for his grant (SFRH/BPD/90562/2012).

Appendix A. Supplementary data

Supplementary data related to this article can be found at http://dx.doi.org/10.1016/j.carbon.2017.04.067.

References

[1] X. Wu, Y. Hu, M. Ruan, N.K. Madiomanara, J. Hankinson, M. Sprinkle, C. Berger, W.A. de Heer, Half integer quantum Hall effect in high mobility single layer epitaxial graphene, Appl. Phys. Lett. 95 (2009) 223108.
[2] A.C. Ferrari, F. Bonaccorso, V. Fal'ko, K.S. Novoselov, S. Roche, P. Bøggild, et al., Science and technology roadmap for graphene, related two-dimensional crystals, and hybrid systems, Nanoscale 7 (2015) 4598.
[3] K.S. Novoselov, A.K. Geim, S.V. Morozov, D. Jiang, Y. Zhang, S.V. Dubonos, I.V. Grigorieva, A.A. Firsov, Electric field effect in atomically thin carbon films, Science 306 (2004) 666.
[4] A.H. Castro Neto, F. Guinea, N.M.R. Peres, K.S. Novoselov, A.K. Geim, The electronic properties of graphene, Rev. Mod. Phys. 81 (2009) 109.
[5] C. Lee, X. Wei, J.W. Kysar, J. Hone, Measurement of the elastic properties and intrinsic strength of monolayer graphene, Science 321 (2008) 385.
[6] X. Li, W. Cai, J. An, S. Kim, J. Nah, D. Yang, et al., Large-area synthesis of high-quality and uniform graphene films on copper foils, Science 324 (2009) 1312.
[7] Y. Hernandez, V. Nicolosi, M. Lotya, F.M. Blighe, Z. Sun, S. De, et al., High-yield production of graphene by liquid-phase exfoliation of graphite, Nat. Nanotechnol. 3 (2008) 563.
[8] Q. Yu, J. Lian, S. Siriponglert, H. Li, Y.P. Chen, S. Pei, Graphene segregated on Ni surfaces and transferred to insulators, Appl. Phys. Lett. 93 (2008) 113103.
[9] W. Norimatsu, M. Kusunoki, Epitaxial graphene on SiC{0001}: advances and perspectives, Phys. Chem. Chem. Phys. 16 (2014) 3501.
[10] R. Muñoz, C. Gomez-Aleixandre, Review of CVD synthesis of graphene, Chem. Vap. Depos. 19 (2013) 297.
[11] H.W. Kroto, J.R. Heath, S.C. ÓBrien, R.F. Curl, R.E. Smalley, C60: buckminsterfullerene, Nature 318 (1985) 162.
[12] C.S. Sundar, A. Bharathi, Y. Hariharan, J. Janaki, V.S. Sastry, T.S. Radhakrishnan, Thermal decomposition of C_{60}, Solid State Comm. 84 (1992) 823.
[13] L.M.A. Perdigao, S.N. Sabki, J.M. Garfitt, P. Capiod, P.H. Beton, Graphene formation by decomposition of C60, J. Phys. Chem. C 115 (2011) 7472.
[14] Y. Yamada, S. Yamada, T. Nakayama, M. Sasaki, T. Tsuru, Electronic modification of C60 monolayers via metal substrates, Jpn. J. Appl. Phys. 50 (2011) 08LB06.
[15] J. Lu, P.S.E. Yeo, C.K. Gan, P. Wu, K.P. Loh, Transforming C60 molecules into graphene quantum dots, Nat. Nanotechnol. 6 (2011) 247.
[16] X. Fei, X. Zhang, V. Lopez, G. Lu, H.J. Gao, L. Gao, Strongly interacting C60/Ir(111) interface: transformation of C60 into graphene and influence of graphene interlayer, J. Phys. Chem. C 119 (2015) 27550.
[17] R. Felici, M. Pedio, F. Borgatti, S. Iannotta, M. Capozi, G. Ciullo, A. Stierle, X-ray-diffraction characterization of Pt(111) surface nanopatterning induced by C60 adsorption, Nat. Mater. 4 (2005) 688.
[18] G. Otero, C. González, A.L. Pinardi, P. Merino, S. Gardonio, S. Lizzit, et al., Ordered vacancy network induced by the growth of epitaxial graphene on Pt(111), Phys. Rev. Lett. 105 (2010) 216102.
[19] R. Tatti, L. Aversa, R. Verucchi, E. Cavaliere, G. Garberoglio, N.M. Pugno, G. Speranza, S. Taioli, Synthesis of single layer graphene on Cu(111) by C60 supersonic molecular beam epitaxy, RSC Adv. 6 (2016) 37982.
[20] I. Horcas, R. Fernandez, J.M. Gomez-Rodriguez, J. Colchero, J. Gomez-Herrero, A.M. Baro, WSXM: a software for scanning probe microscopy and a tool for nanotechnology, Rev. Sci. Instrum. 78 (2007) 013705.
[21] www.next-tip.com.
[22] L. Aballe, M. Foerster, E. Pellegrin, J. Nicolas, S. Ferrer, The ALBA spectroscopic LEEM-PEEM experimental station: layout and performance, J. Synch. Rad. 22 (2015) 745.
[23] M. Lazzeri, F. Mauri, First-Principles calculation of vibrational Raman spectra in large systems: signature of small rings in crystalline SiO2, Phys. Rev. Lett. 90 (2003) 036401.
[24] P. Giannozzi, S. Baroni, N. Bonini, M. Calandra, R. Car, C. Cavazzoni, et al., Quantum espresso: a modular and open-source software project for quantum simulations of materials, J. Phys. Cond. Matt. 21 (2009) 395502.
[25] P. Giannozzi, S. de Gironcoli, P. Pavone, S. Baroni, Ab initio calculation of phonon dispersions in semiconductors, Phys. Rev. B 43 (1991) 7231.
[26] X. Gonze, Adiabatic density-functional perturbation theory, Phys. Rev. A 52 (1995) 1096.
[27] P. Brüesch, Phonons: Theory and Experiments II, Springer, Berlin, 1986.
[28] S. Baroni, S. de Gironcoli, A. Dal Corso, P. Giannozzi, Phonons and related crystal properties from density-functional perturbation theory, Rev. Mod. Phys. 73 (2001) 515.
[29] X. Gonze, C. Lee, Dynamical matrices, born effective charges, dielectric permittivity tensors, and interatomic force constants from density-functional perturbation theory, Phys. Rev. B 55 (1997) 10355.
[30] A. Calzolari, M.B. Nardelli, Dielectric properties and Raman spectra of ZnO from a first-principles finite-differences/finite-fields approach, Sci. Rep. 3 (2013) 2999.
[31] V. Barone, M. Casarin, D. Forrer, M. Pavone, M. Sambi, A. Vittadini, Role and effective treatment of dispersive forces in materials: polyethylene and graphite crystals as test cases, J. Comput. Chem. 30 (2009) 934.
[32] S. Grimme, Semiempirical GGA-type density functional constructed with a long-range dispersion correction, J. Comp. Chem. 27 (2006) 1787.
[33] J.P. Perdew, K. Burke, M. Ernzerhof, Generalized gradient approximation made simple, Phys. Rev. Lett. 77 (1996) 3865.
[34] N. Troullier, J.L. Martins, Efficient pseudopotentials for plane-wave calculations, Phys. Rev. B 43 (1991) 1993.
[35] H.J. Monkhorst, J.D. Pack, Special points for brillouin-zone integrations, Phys. Rev. B 13 (1976) 5188.
[36] A.L. Pinardi, G. Biddau, K. van De Ruit, G. Otero, S. Gardonio, M. Blanco-Rey, et al., Vacancy formation on C60/Pt(111): unraveling the complex atomistic mechanism, Nanotechnology 25 (2014) 385602.
[37] J. Avila, I. Razado, S. Lorcy, R. Fleurier, E. Pichonat, D. Vignaud, X. Wallart, M.C. Asensio, Exploring electronic structure of one-atom thick polycrystalline graphene films: a nano angle resolved photoemission study, Sci. Rep. 3 (2013) 2439.
[38] A.Y. Lu, S.Y. Wei, C.Y. Wu, Y. Hernandez, T.Y. Chen, T.H. Liu, C.W. Pao, F.R. Chen, L.J. Li, Z.Y. Juang, Decoupling of CVD graphene by controlled oxidation of recrystallized Cu, RSC Adv. 2 (2012) 3008.
[39] O. Frank, J. Vejpravova, V. Holy, L. Kavan, M. Kalbac, Interaction between graphene and copper substrate: the role of lattice orientation, Carbon 68 (2014) 440.
[40] G.V. Bianco, M. Losurdo, M.M. Giangregorio, P. Capezzuto, G. Bruno, Exploring and rationalising effective n-doping of large area CVD-graphene by NH3, Phys. Chem. Chem. Phys. 16 (2014) 3632.
[41] S.R. Na, J.W. Suk, L. Tao, D. Akinwande, R.S. Ruoff, R. Huang, K.M. Liechti, Selective mechanical transfer of graphene from seed copper foil using rate effects, ACS Nano 9 (2015) 1325.
[42] G.A. Lopez, E.J. Mittemeijer, The solubility of C on solid Cu, Scr. Mater. 51 (2004) 1.
[43] K.C. Prince, I. Ulrych, M. Peloi, B. Ressel, Core-level photoemission from graphite, Phys. Rev. B 62 (2000) 6866.
[44] Q. Zhou, S. Coh, M.L. Cohen, S.G. Louie, A. Zettl, Imprint of transition metal d orbitals on a graphene Dirac cone, Phys. Rev. B 88 (2013) 235431.
[45] X. Yin, Y. Li, F. Ke, C. Lin, H. Zhao, L. Gan, et al., Evolution of the Raman spectrum of graphene grown on copper upon oxidation of the substrate, Nano Res. 7 (2014) 1613.
[46] R. Ramírez-Jimenez, L. Alvarez-Fraga, F. Jimenez-Villacorta, E. Climent-Pascual, C. Prieto, A. de Andrés, Interference enhanced Raman effect in graphene

bubbles, Carbon 105 (2016) 556.
[47] R. Wu, L. Gan, X. Ou, Q. Zhang, Z. Luo, Detaching graphene from copper substrate by oxidation-assisted water intercalation, Carbon 98 (2016) 138.
[48] A.C. Ferrari, J.C. Meyer, V. Scardaci, C. Casiraghi, M. Lazzeri, F. Mauri, et al., Raman spectrum of graphene and graphene layers, Phys. Rev. Lett. 97 (2006) 187401–187404.
[49] Z.H. Ni, T. Yu, Y.H. Lu, Y.Y. Wang, Y.P. Feng, Z.X. Shen, Uniaxial strain in graphene: Raman spectroscopy study and band-gap opening, ACS Nano 2 (2008) 2301.
[50] J.I. Martinez, P. Merino, A.L. Pinardi, G. Otero-Irurueta, M.F. Lopez, J. Mendez, J.A. Martin-Gago, Role of the pinning points in epitaxial graphene Moiré superstructures on the Pt (111) surface, Sci. Rep. 6 (2016) 20354.
[51] G. Fisichella, S. Di Franco, P. Fiorenza, R. Lo Nigro, F. Roccaforte, C. Tudisco, et al., Micro- and nanoscale electrical characterization of large-area graphene transferred to functional substrates, Beilstein J. Nanotechnol. 4 (2013) 234.
[52] H. Vita, S. Böttcher, K. Horn, E.N. Voloshina, R.E. Ovcharenko, Th Kampen, A. Thissen, Y.S. Dedkov, Understanding the origin of band gap formation in graphene on metals: graphene on Cu/Ir(111), Sci. Rep. 4 (2014) 5704.
[53] M. Bruna, A.K. Ott, M. Ijäs, D. Yoon, U. Sassi, A.C. Ferrari, Doping dependence of the raman spectrum of defected graphene, ACS Nano 8 (2014) 7432.
[54] H. Gonzalez-Herrero, P. Pou, J. Lobo-Checa, D. Fernandez-Torre, F. Craes, A.J. Martinez-Galera, et al., Graphene tunable transparency to tunneling electrons: a direct tool to measure the local coupling, ACS Nano 10 (2016) 5131.
[55] A.J. Marsden, M.C. Asensio, J. Avila, P. Dudin, A. Barinov, P. Moras, et al., Is graphene on copper doped? Phys. Status Solidi RRL 7 (2013) 643.